The Thermal, Magnetic, and Structural Characterization of the Crystallization Kinetics of $Fe_{88}Zr_7B_4Cu_1$, An Amorphous Soft Magnetic Ribbon

A. Hsiao, M. E. McHenry, D. E. Laughlin, M. J. Kramer, C. Ashe, and T. Ohkubo

***Abstract*—The characterization of the crystallization kinetics of an amorphous soft magnetic alloy, $Fe_{88}Zr_7B_4Cu_1$, called NANOPERM, is presented. Vibrating sample magnetometry (VSM), X-ray diffractometry, and differential scanning calorimetry have been used to observe crystallization kinetics. The VSM observations take advantage of the Curie temperature of the amorphous phase $T_{c,amorphous}$ of the NANOPERM alloy being below its primary crystallization temperature T_{x1}. This allows for the volume of nanocrystals transformed in the crystallization process to be inferred magnetically, as well as thermally and structurally. The Johnson–Mehl–Avrami model for isothermal crystallization kinetics is compared with the Kissinger model for nonisothermal crystallization kinetics using data gathered from the three characterization methods. Linear regression and nonlinear regression analysis of crystallization data for NANOPERM ribbon and the significance of the values that describe them, namely, the activation energy Q and the morphology index n are investigated for isothermal and constant-heating crystallization. The activation energy for NANOPERM ribbon is presented here to be in the range of $Q = 2.8$–3.4 eV, with the crystallization kinetics proceeding by three-dimensional diffusion and immediate nucleation, where the morphology index is $n = 1.5$. A time constant to account for initial nonisothermal conditions during isothermal heating is introduced and determined to be $\tau = 120$–200 s.**

***Index Terms*—Activation energy, crystallization kinetics, differential scanning calorimetry, NANOPERM, vibrating sample magnetometry, X-ray diffractometry.**

I. Introduction

THE understanding of the crystallization kinetics of magnetic amorphous alloys is of scientific interest for two important reasons. First of all, for the case of an alloy that exhibits excellent magnetic properties in its amorphous phase, the crystallization kinetics represents the limit at which these properties begin to deteriorate. Therefore, thermal stability determines the magnetic stability of the amorphous phase of the material. Second, for the case of alloys that exhibit excellent magnetic properties in the two-phase nanocrystal-amorphous matrix structure, control over the crystallization kinetics allows for the ability to tailor the microstructure. The amount of nanocrystals formed within the matrix can be controlled to achieve the desired magnetic performance. The modes of crystallization from the metastable amorphous state to the stable crystalline state depend on various parameters, such as the composition, the concentration of nucleation sites, diffusion coefficients, the activation energy for diffusion, the free-energy difference between amorphous and crystalline phases, and the thermal history of the sample.

Manuscript received February 12, 2002; revised April 28, 2002. This work was supported by the National Science Foundation under Grant DMR-9803700, by the Air Force Office of Scientific Research, Air Force Material Command, U.S. Air Force, under Grant 49620-96-1-0454, and by ABB Corporation. The work of M. J. Kramer was supported by the U.S. Department of Energy through Iowa State University under Contract W-7405-ENG-82. Use of the Advanced Photon Source, MUCAT, was supported by the U.S. Department of Energy, Basic Energy Sciences, Office of Science, under Contract W-31-109-Eng-38.

A. Hsiao is with SATIE UMR-CNRS, Ecole Normale Supérieure de Cachan, 94235 Cachan Cedex, France (e-mail: amyhsiao@alum.mit.edu).

M. E. McHenry, D. E. Laughlin, C. Ashe, and T. Ohkubo are with the Department of Materials Science and Engineering, Carnegie Mellon University, Pittsburgh, PA 15213 USA (e-mail: mm7g@andrew.cmu.edu; dl0p@andrew.cmu.edu; okubo@cmu.edu).

M. J. Kramer is with the Department of Materials Science and Engineering and Ames Laboratory, Iowa State University, Ames, IA 50011 USA (e-mail: mjkramer@ameslab.gov).

Digital Object Identifier 10.1109/TMAG.2002.802434.

II. Modes of Crystallization and Free Energy

A. Polymorphous, Primary, and Eutectic Crystallization

In metallic glasses, there are three important modes of crystallization that have been found to occur by nucleation and growth processes, depending on the composition of a particular alloy. **Polymorphous crystallization** describes the crystallization of an amorphous phase to a crystalline one without any change in the composition of that phase. There is no concentration difference across the reaction front because the concentration does not change. **Primary crystallization** describes the crystallization of an amorphous alloy in which a phase of one of the alloy constituents is first to crystallize. This dispersed primary crystallized phase coexists with the amorphous matrix and may serve as the nucleation site for secondary or tertiary crystallization. The concentration profile in the crystallizing phase is high at the interface of the nanocrystal. **Eutectic crystallization** is the simultaneous crystallization of two crystalline phases by a discontinuous reaction. This reaction has no concentration difference across the reaction front, but takes longer than polymorphous crystallization to proceed because the two components have to separate by diffusion into two separate phases within the crystallized region.

B. Change in Free Energy for the Fe–Zr Binary System

The Fe–Zr alloy system has an eutectic composition that is close to the pure transition metal composition, i.e., that of a high

0018-9464/02$17.00 © 2002 IEEE

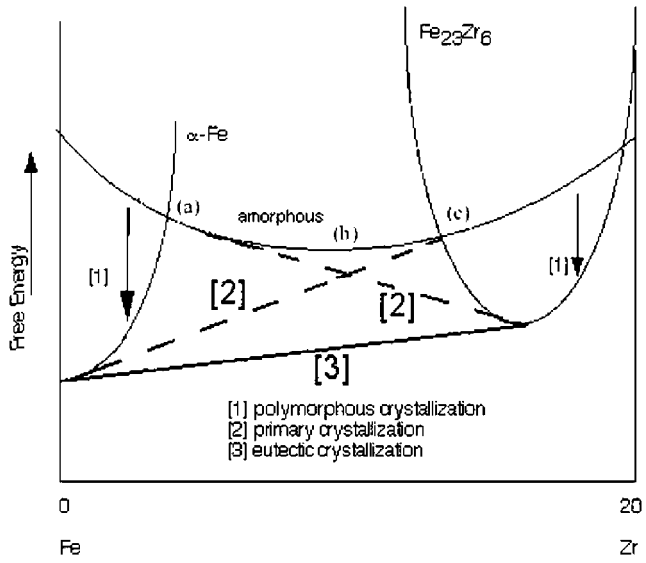

Fig. 1. Free-energy curves illustrating polymorphous [1], primary [2], and eutectic [3] crystallization of Fe–Zr.

Fe content. This means that the alloy can maintain the highest induction and can be quenched to directly obtain an amorphous structure. Zr serves as a glass forming element, and its large atomic size can be expected to affect the interaction with Fe and the mechanism for diffusion. When Fe–Zr liquid is quenched to its metastable amorphous phase, α-Fe is the first to crystallize in the two-phase region. The kinetic steps of crystallization for the eutectic composition of rapidly quench amorphous $Fe_{90.2}Zr_{9.8}$ can then be described as

$$\begin{aligned} Fe_{90.2}Zr_{9.8}\ \text{(liquid)} &\rightarrow Fe_{90.2}Zr_{9.8}\ \text{(amorphous)} \\ Fe_{90.2}Zr_{9.8} &\rightarrow \alpha\text{-Fe} + \text{amorphous matrix} \\ &\rightarrow \alpha\text{-Fe} + Fe_{23}Zr_6 + \text{amorphous matrix} \\ &\rightarrow \alpha\text{-Fe} + Fe_{23}Zr_6. \end{aligned}$$

A schematic for the free-energy curves corresponding to the three modes of crystallization is depicted in Fig. 1. Primary crystallization of α-Fe occurs for any composition of x_{Zr} in the region of the amorphous curve marked by points (a) and (b). Secondary crystallization of $Fe_{23}Zr_6$ occurs for a composition of x_{Zr} in the region of the amorphous curve marked by points (b) and (c). These crystallization events are metastable, with the equilibrium composition being a (α-Fe + $Fe_{23}Zr_6$) phase as represented by the line tangent to both the α-Fe and $Fe_{23}Zr_6$ free-energy curves.

III. Models of Crystallization Kinetics

A. Kissinger Model of Crystallization Kinetics

The Kissinger model describes crystallization kinetics during continuous heating. The Kissinger equation

$$\ln\left(\frac{\phi}{T_p^2}\right) = -\frac{Q_K}{RT_p} + \text{constant} \tag{1}$$

relates the natural log of the heating rate ϕ and the peak temperature T_p to the activation energy Q_K, the ideal gas constant R, and T_p. The activation energy Q_K allows for the energy barrier opposing the phase transformation to be quantitatively described. The peak temperature T_p refers to the change in heat content due to the change in the thermal properties of the sample when a reaction occurs in differential thermal calorimetry. Kissinger first established that the peak temperature T_p was dependent on the heating rate ϕ, and that the variation in T_p could be used to determine the activation energy Q_K for first-order reactions. He later extended this to apply to reactions of any order [1].

B. Johnson–Mehl–Avrami Model

The Johnson–Mehl–Avrami (JMA) model describes the crystallization kinetics during an isothermal process. The JMA rate equation is derived assuming that the following conditions apply.

1) Nucleation and growth occur at a constant temperature, i.e., isothermal crystallization.
2) Nucleation is random throughout the bulk of the sample, which is assumed to be infinite.
3) Growth is isotropic until crystals impinge upon one another.

The JMA equation is sometimes rederived to match specific experimental conditions if these conditions are not satisfied. The volume fraction transformed during crystallization is written as

$$X(t) = 1 - \exp[-(kt)^n] \tag{2}$$

in which the volume fraction transformed, X, as a function of time t is related to the rate constant k, time t, and the morphology index n. The value of the morphology index is indicative of the dimensionality of, and the mechanism responsible for, the phase transformation occurring during crystallization. The rate constant can be written as

$$k(T) = k_{\text{JMA}}^{o} \exp\left(\frac{-Q_{\text{JMA}}}{RT}\right) \tag{3}$$

where k_{JMA}^{o} is the rate constant coefficient and Q_{JMA} is the activation energy. Given the JMA model and the Kissinger model, it is of interest to compare the activation energies Q of each. The morphology index, also known as the Avrami exponent n, calculated from isothermal experiments on the vibrating sample magnetometry (VSM) and the differential scanning calorimetry (DSC) can be compared also.

C. Nucleation and Growth Kinetics

The fundamental importance of these empirical transformation kinetics lies in coupling them with a model for nucleation and growth. The morphology index n can be compared with model-specific predictions of nucleation and growth kinetics in which particle geometry is considered, as shown in Table I. Other values of n are possible, for example, if the growth is not of spherical particles. These experimental values serve to describe the kinetics quantitatively.

IV. Experimental Analysis of Crystallization Kinetics

A. Via Differential Scanning Calorimetry

Six sets of NANOPERM ribbon were prepared, each with a weight of 10 mg $\pm$ 2 mg. A heating rate was assigned to each sample, resulting in six different heating rates to be tested: 2 °C/min, 5 °C/min, 10 °C/min, 20 °C/min, 40 °C/min, and

TABLE I
NUCLEATION TYPES AND ASSOCIATED GROWTH GEOMETRIES AND MORPHOLOGY INDICES n

Nucleation Type	Growth Geometry	(n) for chemical reaction (linear law)	(n) for diffusion (parabolic law)
Instantaneous	Bulk 1-D growth	1	1/2
Nucleation (site	Bulk 2-D growth	2	1
Saturation)	Bulk 3-D growth	3	3/2
Constant Rate	Bulk 1-D growth	2	3/2
Homogeneous	Bulk 2-D growth	3	2
Nucleation	Bulk 3-D growth	4	5/2

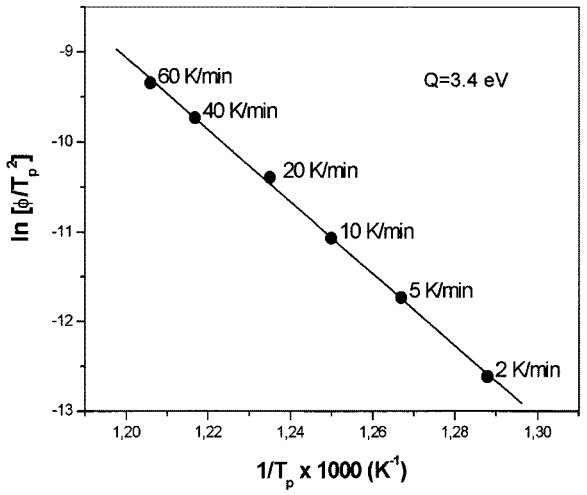

Fig. 2. Kissinger plot of NANOPERM crystallization. The activation energy Q is 3.4 eV.

60 °C/min. Each sample was heated from 50 °C to 580 °C. It was shown that the peak temperature $T_{\rm p}$ increases as the heating rate increases [2], suggesting a dependence of $T_{\rm p}$ on the heating rate of the sample. The temperature dependence of $T_{\rm p}$ on the heating rate demonstrates that the Kissinger model of transformation can be used to relate the rate of heating to the activation energy and temperature. The activation energy from the Kissinger model was calculated to be 3.4 eV as shown in Fig. 2. This is the fitted value for the slope of a Kissinger plot, where the regression coefficient was $R^2 = 0.999$.

B. Via Vibrating Sample Magnetometry

NANOPERM alloy has essentially zero magnetization when heated to its crystallization temperature after passing its amorphous Curie temperature, as seen in Fig. 3. As the alloy crystallizes, the magnetization is directly proportional to the volume fraction of body-centered cubic (BCC) α-Fe that forms. Thus, the volume fraction transformed can be determined as a fraction of time, since it is directly related to the magnetization of the sample, making VSM an excellent method for observing crystallization kinetics.

Six samples of $Fe_{88}Zr_7B_4Cu_1$ NANOPERM ribbon were prepared and heated at an isothermal temperature ranging from 490 °C for 4 h, 500 °C for 4 h, 510 °C for 4 h, 520 °C for 3 h, 550 °C for 2 h, and 570 °C for 1 h. The magnetization of each curve was normalized to the saturation magnetization

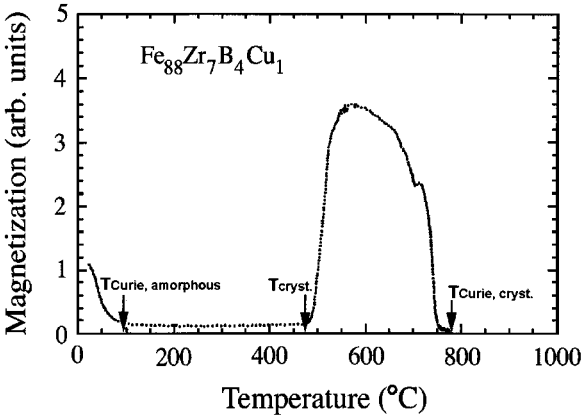

Fig. 3. Magnetization versus temperature for NANOPERM ribbon.

at a saturation time of 2 h for the isothermal temperatures of 490 °C, 500 °C, and 510 °C, and a saturation time of 1 h for isothermal temperatures of 520 °C, 550 °C, and 570 °C. From each curve, it was seen that the crystallization transformation occurred gradually, after an initial incubation time, at isothermal temperatures lower than 510 °C. At isothermal temperatures greater than 510 °C, it was observed that the reaction occurred immediately. The presence of an incubation time at lower temperatures suggests that a mathematical time constant needed to be considered. This time constant would also account for the presence of initial nonisothermal conditions in all runs at all temperatures.

1) Linear Regression Analysis of JMA Isothermal Data to Determine the Activation Energy $Q_{\rm JMA}$: The JMA equation can be written with time t as the dependent variable, where t is chosen from the experimental data. In this case, t is chosen as the time where the inflection of each M versus time isothermal curve occurs. Thus, $t_{\rm inf}$ is the time at which dM/dt (inferred dX/dt) is a maximum and

$$\ln(t_{\rm inf}) = \frac{Q_{\rm JMA}}{RT} \tag{4}$$

where $Q_{\rm JMA}$ is the activation energy for the JMA model, R is the ideal gas constant, and T is the temperature of the sample [3]. Initial analysis using a linear regression fit to the line of $\ln(t_{\rm inf})$ as a function of $1/T$ showed a poor fit, with a regression coefficient of $R^2 = 0.95$. This suggested that a time constant τ needed to be considered for each isothermal experiment to mathematically account for the physical representation of the time needed for the sample to heat up to and match the experimental temperature. It is not negligible, or immediate, for isothermal runs at higher temperatures, namely, at 550 °C and 570 °C. Linear regression fits with $\tau = 60$ s, $\tau = 80$, and $\tau = 100$ s at all six isothermal runs showed that, indeed, the time constant had significant importance at higher temperatures. However, a time constant of $\tau \geq 100$ s, when the time maximum rate of volume transformed at 570 °C, is 120 s, indicates that a run at 570 °C does not proceed entirely under isothermal conditions. A series of linear regression fits were performed again on the isothermal runs of 490 °C, 500 °C, 510 °C, 520 °C, and 550 °C only. A linear regression fit for $\tau = 60$ s, $\tau = 80$ s, $\tau = 100$ s, $\tau = 120$ s, $\tau = 160$ s, and $\tau = 200$ s showed that the value for the activation energy increased and

the linear regression coefficients increased systematically with increasing time constant. The time constant with the best fit was 200 s. Similarly, a time constant greater than 60 s, when the t_{inf} at 550 °C is 227 s, indicates that the kinetics at 550 °C are not entirely at isothermal conditions, and the data cannot be considered in the analyses.

Linear regression fits to the three lowest isothermal temperatures were performed. The linear regression fit for $\tau = 0$ for temperatures 490 °C, 500 °C, and 510 °C showed the best fit with a regression coefficient of $R^2 = 0.98$ and a calculated activation energy Q_{JMA} of 3.4 eV. The linear regression fit for temperatures 490 °C, 500 °C, and 520 °C with a time constant of $\tau = 200$ s showed the best fit, with a regression coefficient of $R^2 = 0.99$ and a calculated activation energy Q_{JMA} of 3.0 eV. Thus, taking the best fit value for $Q_{\text{JMA,LIN}}$ from the two three-point fits, the activation energy for JMA isothermal crystallization kinetics is experimentally determined for NANOPERM to be in the range of $Q_{\text{JMA}} = 3.0$–3.4 eV, when a time constant of $0 < \tau < 200$ s is included. A heating time of several minutes is reasonable to expect, however, a precise heating time constant is difficult to model. As a result, this time constant is used as a fitting parameter in the JMA model and aimed at ascertaining the activation energy of crystallization.

2) Linear Regression Analysis of JMA Isothermal Data to Determine the Morphology Index n: Given X_{inf} from the VSM data, the value of the morphology index n can be determined from differentiation of the JMA equation with respect to time such that

$$\frac{dX}{dt} = kn(kn)^{n-1}\exp[-(kt)^n]. \tag{5}$$

Substitution of $(1 - X)$ for $[\exp(-(kt)^n]$ yields

$$\frac{dX}{dt} = kn(kn)^{n-1}[1 - X]. \tag{6}$$

The second derivative of this equation results in

$$\frac{d^2X}{dt^2} = n(n-1)k^2(kt)^{n-2}[1-X] + kn(kt)^{n-1}\left(-\frac{dX}{dt}\right).$$

Substituting $dX/\mathrm{dt} = \mathrm{kn}(kt)^{n-1}[1-X]$ and setting the second dervative to zero results in

$$n(n-1)k^2(kt)^{n-2} = n^2k^2(kt)^{n-1}(1-X)(kt)^{n-1}. \tag{7}$$

Cancellation of exact terms from both sides of the equation results in

$$\frac{n-1}{n} = (kt)^n. \tag{8}$$

Substitution of (8) into (2) and rewriting the volume fraction transformed X in terms of the morphology index n yields

$$X_{\text{inf}} = 1 - \exp\left(-\frac{(n-1)}{n}\right). \tag{9}$$

This equation shows that the isothermal kinetics at the maximum transformation rate are a function of the morphology index n only, and the volume fraction transformed at this maximum rate will be the same for a given set of samples of a material. Table II shows the values of n as calculated from the experimental value of X_{inf}. The morphology index, as determined from linear regression analysis of JMA isothermal crystallization kinetics, is in the range $n = 1.4$–1.6.

TABLE II
MORPHOLOGY INDEX FROM LINEAR REGRESSION ANALYSIS OF JMA CRYSTALLIZATION KINETICS FOR NANOPERM

Temperature (K)	X_{inf}	Morphology index (n)
763 (490°C)	0.33±0.20	1.6±0.3
773 (500°C)	0.27±0.05	1.5±0.1
783 (510°C)	0.25±0.04	1.4±0.1
793 (520°C)	0.33±0.04	1.6±0.1
823 (550°C)	0.33±0.06	1.6±0.1

TABLE III
KINETIC PARAMETERS FROM NONLINEAR REGRESSION ANALYSIS OF JMA ISOTHERMAL DATA ON NANOPERM

	490°C	500°C	510°C	520°C
	(n) morphology index			
τ=0 sec	1.95	1.68	1.27	1.79
τ=90 sec	1.88	1.58	1.13	1.52
τ=120 sec	1.85	1.55	1.08	1.43
τ=150 sec	1.81	1.48	X	X
τ=180 sec	1.80	1.48	X	X
τ=210 sec	1.77	1.45	X	X
τ=421 sec	1.56	X	X	X
	(k) rate constant			
τ=0 sec	$3.2\text{x}10^{-4}$	$5.0\text{x}10^{-4}$	$8.6\text{x}10^{-4}$	$1.2\text{x}10^{-3}$
τ=90 sec	$3.3\text{x}10^{-4}$	$5.0\text{x}10^{-4}$	$9.4\text{x}10^{-4}$	$1.4\text{x}10^{-3}$
τ=120 sec	$3.0\text{x}10^{-4}$	$5.0\text{x}10^{-4}$	$9.7\text{x}10^{-4}$	$1.4\text{x}10^{-3}$
τ=150 sec	$3.3\text{x}10^{-4}$	$5.1\text{x}10^{-4}$	X	X
τ=180 sec	$3.3\text{x}10^{-4}$	$5.2\text{x}10^{-4}$	X	X
τ=210 sec	$3.4\text{x}10^{-4}$	$5.3\text{x}10^{-4}$	X	X
τ=421 sec	$3.7\text{x}10^{-4}$	X	X	X

3) Nonlinear Regression (NLR) Analysis of Isothermal Data to Determine Morphology Index n and Activation Energy $Q_{\text{JMA,NLR}}$: Table III summarizes the values of morphology index n and rate constant k at seven different time constants selected from a systematic analysis for NLR fits at 490 °C, 500 °C, 510 °C, and 520 °C. The NLR fits to isothermal data at 570 °C and 550 °C were imprecise ($R^2 < 0.97$) and resulted in inconsistent values of n. Therefore, the reaction at 570 °C and 550 °C were determined to occur too quickly for the data to be included in the collective analysis. It can be seen from Table III that the best NLR fit for these four isothermal experiments occurs for a time constant of $\tau = 120$ s.

Figs. 4 and 5 show the curves of the JMA equation and the NLR fit with a 120-s time constant plotted to the data for 500 °C and 520 °C, respectively.

It can be seen from these curves and systematic NLR fits that for a time constant of 120 s, the nonlinear fits are very precise. The morphology index n is averaged to be 1.5 and within the range $n = 1.08$–1.85. Fig. 6 shows the plot of $\ln k$ as a function of temperature, $1/T$. The slope of this line is the activation energy. Using the values of the rate constants k determined from the NLR analysis for each isothermal temperature with a time constant of 120 s, the activation energy was determined to be

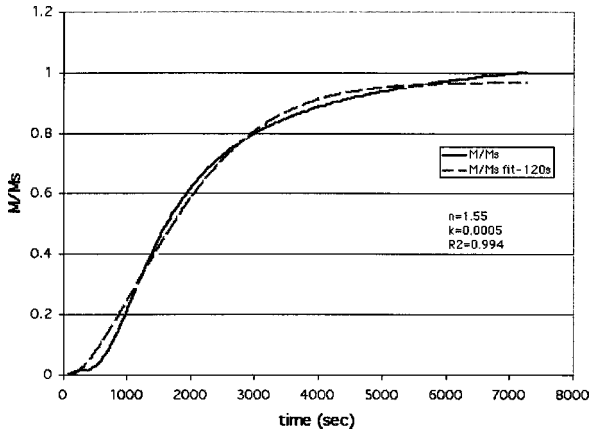

Fig. 4. NLR fit to the JMA curve for 500 °C. The fit includes a 120-s time constant. $R^2 = 0.99$, $k = 0.0005$, and $n = 1.55$.

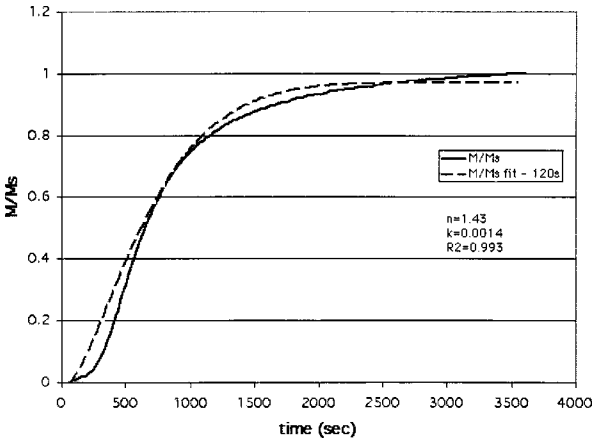

Fig. 5. NLR fit to the JMA curve for 520 °C. The fit includes a 120-s time constant. $R^2 = 0.99$, $k = 0.000\,14$, and $n = 1.43$.

2.8 eV. The rate constant k does not vary with the time constant and is only dependent upon temperature.

The excellent NLR fits to the NANOPERM data still show slight deviations from the JMA function. The observation that these residuals are not random suggests that they are either due to systematic experimental error, to the precision of the current JMA model, or to the presence of mixed kinetics, i.e., that of both bulk and surface diffusion during the crystallization process. The latter is not unreasonable for melt-spun ribbon because the dull side of the ribbon (wheel side) often differs from the microstructure of the shiny side of the ribbon (away from wheel). Compositional inhomogeneities can cause nonrandom nucleation, and surface nanocrystals can form if the nucleation sites are more prevalent at the surface of the ribbon than in the bulk.

C. Time-Resolved X-Ray Diffraction

Synchrotron radiation has been shown to be an excellent source for high-resolution powder diffraction studies. By using a newly designed high-temperature furnace coupled with a sample rotation apparatus [4], changes in the diffraction pattern are obtained in *real time*, corresponding to the phase transformations that occur during the crystallization process.

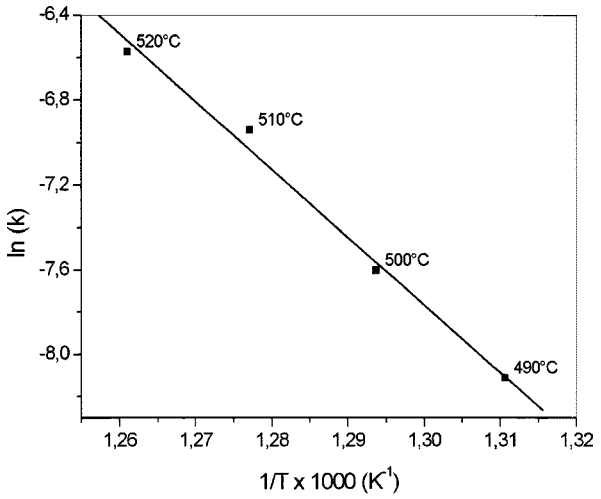

Fig. 6. Activation energy $Q_{\mathrm{JMA,NLF}}$ is determined from the slope of this curve plotting $\ln k$ as a function of $1/T(K^{-1})$. The rate constant k is determined from NLR fits (with a 120-s time constant) to isothermal data. $Q_{\mathrm{JMA,NLF}} = 2.8$ eV.

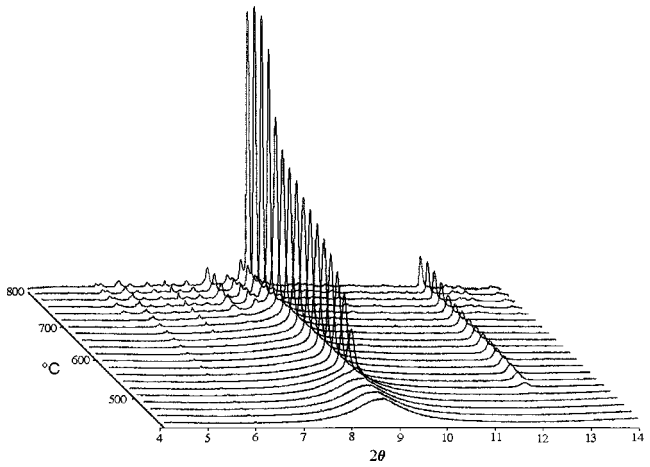

Fig. 7. Three-dimensional synchrotron diffraction patterns of α-Fe from 400 °C to 800 °C, showing the transformation from amorphous to crystalline, first and second crystallization phases, and the growth and coarsening phenomena of NANOPERM crystallization kinetics.

As a result, the amorphous-to-crystalline transition is clearly observed by this method, as well as the appearance and identification of nanocrystalline phases.

Fig. 7 illustrates the characteristics of the crystallization transformations of NANOPERM ribbon.

1) The sharpening of the Fe(110) peak is apparent as the transformation of amorphous to crystalline phase occurs.
2) Primary crystallization of α-Fe is confirmed with the appearance of the Fe(200) peak at $T_{\mathrm{x1}} \sim 510$ °C.
3) T_{x2} occurs at ~ 710 °C with the crystallization of $Fe_{23}Zr_6$.

Secondary crystallization of $Fe_{23}Zr_6$ is seen in Fig. 8. Well after $T_{\mathrm{x2}} \sim 715$ °C, distinct peaks of $Fe_{23}Zr_6$ appear. These peaks are not present below T_{x2}. The appearance of $Fe_{23}Zr_6$, instead of Fe_3Zr, confirm the nonequilibrium characteristic of crystallization.

Transmission electron microscopy of the NANOPERM ribbon taken after being heated to 800 °C confirms the presence

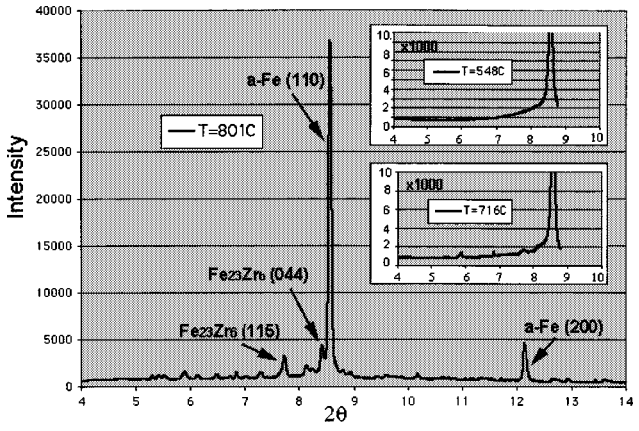

Fig. 8. Synchrotron radiation diffraction pattern of secondary crystallization of $Fe_{23}Zr_6$ of NANOPERM. At 546 °C, only sharp intensity peaks are present for α-Fe. The onset of secondary crystallization occurs at 716 °C.

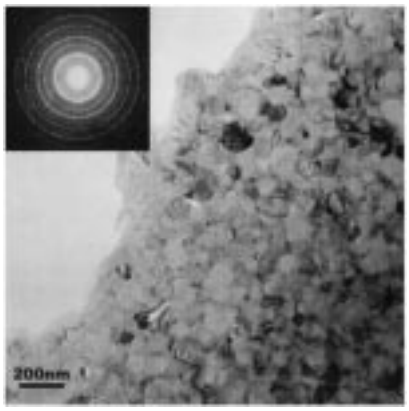

Fig. 9. Bright field transmission electron image of NANOPERM ribbon after heating from 300 °C to 800 °C.

of α-Fe, $Fe_{23}Zr_6$, and Fe_2Zr. The presence of Fe_2Zr suggests that the ribbon composition is not homogeneous and some portions of the ribbon have less than $x = 88$ of Fe. Fig. 9 shows the bright field image confirming the growth and the coarsening inferred by synchrotron analysis.

V. Conclusion

The activation energy for Fe self-diffusion in pure BCC α-Fe is 239.7 kJ/mol or 2.5 eV at atmospheric pressure [6]. However, it can be seen from the experimentally determined higher values of activation energy in both the isothermal and constant-heating kinetics that Zr and B also play a part in the crystallization of NANOPERM. Indeed, Zr also diffuses away from the growing crystals.[1] From the various analyses presented here, the morphology index is concluded to be $n = 3/2$ for NANOPERM, where the reaction is three-dimensionally diffusion limited after initial immediate nucleation. Values of Q and n are comparable with those published in the literature on similar amorphous magnetic alloys. Table IV indicates that kinetic analysis has been done either using the JMA model or the Kissinger model on these alloys, but rarely both.

[1]Activation energy for substitutional self-diffusion of β-Zr is 273.5 kJ/mol or 2.8 eV.

TABLE IV
Activation Energies and Morphology Indices for NANOPERM, FINEMET, and HITPERM, Alloys

Alloy	Analysis	Q(eV)	(n)	Method
$Fe_{87.5}Zr_6B_{5.5}Al_1$	JMA	3.6	1.5	DSC [6]
$Fe_{73.5}Si_{13.5}B_6Nb_3Cu_1$	JMA	4.3	1.5-2.0	DSC[7]
$(FeCo)_{88}Zr_7B_4Cu_1$	Kissinger	3.3	--	DSC [8]

The crystallization kinetics of NANOPERM ribbon were observed thermally, magnetically, and microstructurally by the collective use of the conventional method of differential thermal calorimetry, as well as the novel methods of VSM and time-resolved synchrotron diffractometry. The activation energies using Kissinger and JMA models of crystallization kinetics were found to be similar, and comparable wh values reported in the literature. NLR analysis of the JMA model, along with conventional linear analysis, allowed for a precise depiction of isothermal crystallization kinetics and the mechanisms of crystallization of this amorphous magnetic alloy.

Acknowledgment

The authors would like to thank Dr. V. Harris for providing the NANOPERM ribbon.

References

[1] H. Kissinger, "Reaction kinetics in differential thermal analysis," *Anal. Chem.*, vol. 29, pp. 1702–1706, 1957.
[2] A. Hsiao, Z. Turgut, M. A. Willard, E. Selinger, D. E. Laughlin, M. E. McHenry, and R. Hasagawa, "Crystallization and nanocrystallization kinetics of Fe- and Fe(Co)-based amorphous alloys," in *MRS Symp. Proc.*, vol. 577, 1999, pp. 551–556.
[3] D. E. Laughlin, personal communication and unpublished data, Carnegie Mellon University, Pittsburgh, PA, 2000.
[4] M. J. Kramer, L. Margulies, and R. W. McCallum, "New high temperature furnace for structure refinement by powder diffraction in controlled atmospheres using synchrotron radiation," *Rev. Sci. Instrum.*, vol. 70, no. 9, pp. 3554–3561, 1999.
[5] D. A. Porter and K. E. Easterling, *Phase Transformations in Metals and Alloys*, 2nd ed. London, U.K.: Chapman & Hall, 1992, p. 78.
[6] M. Al-Haj and J. Barry, *J. Mater. Sci. Lett.*, vol. 16, no. 20, pp. 1640–1642, 1997.
[7] J. Bigot *et al.*, *J. Magn. Magn. Mater.*, vol. 133, pp. 299–302, 1994.
[8] M. A. Willard, D. E. Laughlin, M. E. McHenry, D. Thoma, K. Sickafus, J. Cross, and V. G. Harris, *J. Appl. Phys.*, vol. 84, pp. 6773–6777, 1998.